

Understanding the Design of Cathode Materials for Na-Ion Batteries

Priyanka Gupta, Sujatha Pushpakanth, M. Ali Haider, and Suddhasatwa Basu*

Cite This: *ACS Omega* 2022, 7, 5605–5614

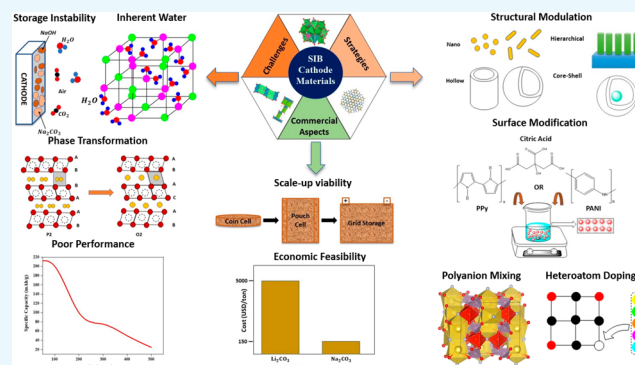
Read Online

ACCESS |

Metrics & More

Article Recommendations

ABSTRACT: With the escalating demand for sustainable energy sources, the sodium-ion batteries (SIBs) appear as a pragmatic option to develop large energy storage grid applications in contrast to existing lithium-ion batteries (LIBs) owing to the availability of cheap sodium precursors. Nevertheless, the commercialization of SIBs has not been carried out so far due to the inefficacies of present electrode materials, particularly cathodes. Thus, from a future application perspective, this short review highlights the intrinsic challenges and corresponding strategies for the extensively researched layered transition metal oxides, polyanionic compounds, and Prussian blue analogues. In addition, the commercial feasibility of existing materials considering relevant parameters is also discussed. The insights provided in the current review may serve as an aid in designing efficient cathode materials for state-of-the-art SIBs.



1. INTRODUCTION

Global concern over climate change and the impediment of fossil fuels has led to the emergence of green and sustainable energy alternatives such as solar, wind, and geothermal sources to render the ever-increasing energy demands of the growing population. To combine these inexhaustible, intermittent energy supplies into the grid effectively, the requirement for an efficient electrical energy storage system (EES) is inevitable. Amid the available energy storage technologies, rechargeable batteries seem to be the most promising technology owing to their environmentally friendly nature, flexibility, and high conversion efficiency.^{1a–d}

At present, lithium-ion batteries (LIBs) due to their superior volumetric and gravimetric energy density and long cycle life are deployed extensively in various electronic applications. However, lithium metal's large-scale demand and scarce attainability raise concerns regarding its role in the sustainable development of grid-scale applications. Apart from LIBs, sodium-ion batteries (SIBs) also follow an intercalation-based “rocking chair” mechanism, in which, during the discharging, Li^+ or Na^+ ions intercalate into the cathode via diffusing through the electrolyte from the electrochemically oxidized anode. Meanwhile, to compensate the positive charge of these incoming ions, electrons move toward the cathode with the passage of an external electrical circuit. To facilitate the charging of ion-based batteries, the above-stated process gets reversed to support the electricity-generating activity. Though SIBs and LIBs share a common working principle, the former one falls behind in terms of energy density and reaction

kinetics due to its higher redox potential of -2.71 V vs SHE for Na^+/Na , heavier ion with 23 g mol^{-1} molecular weight, and larger ionic radius of 1.02 Å in contrast to Li (with a redox potential of -3.01 V, a molecular weight of 6.9 g mol^{-1} and 0.76 Å ionic radius). Despite foregoing drawbacks, SIBs hold an upper hand over their counterpart owing to their inertness to aluminum, making Al a feasible current collector, with a larger ionic radius aiding smooth Na intercalation with a wide range of 3d transition metals along with abundant availability of sodium metal. Moreover, stationary storage applications are largely determined by parameters such as cost-effectiveness and longevity. Hence, SIBs are indicated as a potent alternative for the chosen purpose due to sodium's rich natural abundance, faster charging capability, and wider temperature operability. Furthermore, to establish the commercialization of SIBs, extensive efforts ought to be carried out for the development of economically viable and energy-efficient electrode materials.

In the current scenario, exploration of suitable anode materials for SIBs is predominantly limited by poor initial Coulombic efficiency and cyclability. Most of the anode material research has covered transition metal oxides,

Received: October 16, 2021

Accepted: January 25, 2022

Published: February 11, 2022



Table 1. Summary of Electrochemical Performance of SIB Cathode Materials^a

type	material	synthesis	electrolyte	electrochemical performance	ref	
LTMO	P2-Na _{2/3} Fe _{1/2} Mn _{1/2} O ₂	solid state	1 M NaClO ₄ in PC + FEC	190 mAh g ⁻¹ (12 mA g ⁻¹ , 1.5–4.3 V), 79% (30 cycles), 1C = 260 mA g ⁻¹	5a	
	O3-Na _{0.9} Cu _{0.22} Fe _{0.3} Mn _{0.48} O ₂	solid state	0.8 M NaPF ₆ in PC + 2 vol % FEC	100 mAh g ⁻¹ (0.1C, 2.5–4.05 V), 97% (100 cycles), 1C = 100 mA g ⁻¹	6	
	Al ₂ O ₃ -modified P2-Na _{2/3} Ni _{1/3} Mn _{2/3} O ₂	coprecipitation	1 M NaPF ₆ in PC	142.6 mAh g ⁻¹ (0.05C, 2.3–4.5 V), 54.29% (100 cycles)	7	
	hierarchical columnar NaNi _{0.6} Co _{0.05} Mn _{0.35} O ₂	coprecipitation	0.5 M NaPF ₆ in EMS/FEC (98:2 v/v)	157 mAh g ⁻¹ (0.1C, 1.5–3.9 V), 84% (100 cycles), 1C = 150 mA g ⁻¹	11	
	P2/P3-Na _{0.78} Cu _{0.27} Zn _{0.06} Mn _{0.67} O ₂	sol–gel	1 M NaClO ₄ in EC/PC (1:1)	84 mAh g ⁻¹ (1C, 2.5–4.1 V), 85% (200 cycles)	12	
	Na ₂ RuO ₃	thermal decomposition	1 M NaPF ₆ in EC/DEC (1:1 v/v)	180 mAh g ⁻¹ (30 mA g ⁻¹ , 1.5–4.0 V), 89% (50 cycles), 1C = 150 mA g ⁻¹	13	
polyanion	polythiophene-modified NaFePO ₄	in situ polymerization + sodiation	1 M NaClO ₄ in DEC/PC/EC (1:1:1 v/v)	142 mAh g ⁻¹ (10 mA g ⁻¹ , 2.2–4.0 V), 94% (100 cycles)	15a	
	maricite NaFePO ₄	low-temperature solid state	1 M NaPF ₆ in EC/PC (1:1 v/v)	142 mAh g ⁻¹ (0.05C, 1.5–4.5 V), 95% (200 cycles)	15b	
	Na ₄ Fe ₇ (PO ₄) ₆	spray-drying	1 M NaClO ₄ in EC/DEC/FEC (1:1:0.5 w/w)	66.5 mAh g ⁻¹ (5 mA g ⁻¹ , 1.5–4.2 V), 100% (1000 cycles)	16	
	Na ₃ V(PO ₃) ₃ N/NGO	freeze-drying	1 M NaClO ₄ in EC/PC (1:1 v/v) + 5 vol % FEC	78.9 mAh g ⁻¹ (0.1C, 3.0–4.25 V), 100% (100 cycles), 1C = 80 mA g ⁻¹	17	
	Na ₃ V ₂ (PO ₄) ₂ F ₃	carbothermal reduction	1 M NaClO ₄ in PC	111.6 mAh g ⁻¹ (0.091C, 1.6–4.6 V), 97.6% (50 cycles)	18	
	alluaudite Na ₂ Fe ₂ (SO ₄) ₃	low-temperature solid state	1 M NaPF ₆ in EC/DEC (5:5 v/v)	100 mAh g ⁻¹ (0.05C, 2.0–4.5 V), 91% (30 cycles)	19a	
	eldefellite NaFe(SO ₄) ₂	low-temperature solution route	1 M NaClO ₄ in 10% FEC in PC	80 mAh g ⁻¹ (0.1C, 2.0–4.0 V), 79% (80 cycles)	19b	
	Na ₄ Fe ₃ (PO ₄) ₂ P ₂ O ₇	solid state	1 M NaClO ₄ in PC	129 mAh g ⁻¹ (0.025C, 1.7–4.3 V), 86% (100 cycles)	20a	
		Na _{3.1} V ₂ (PO ₄) _{2.9} (SiO ₄) _{0.1}	sol–gel	1 M NaClO ₄ in PC + 5 vol % FEC	109.4 mAh g ⁻¹ (0.2C, 2.3–3.9 V), 98% (500 cycles)	20b
	PBA	Na _{1.92} Fe ₂ (CN) ₆	solution and washing based route	1 M NaPF ₆ in EC/DEC (1:1 v/v) + 5 wt % FEC	157 mAh g ⁻¹ (10 mA g ⁻¹ , 1.5–4.5 V), 80% (1000 cycles), 1C = 150 mA g ⁻¹	22
Na ₂ Mn _{0.15} Co _{0.15} Ni _{0.1} Fe _{0.6} Fe(CN) ₆		modified coprecipitation	1 M NaClO ₄ in EC/DEC (1:1 v/v) + 8 vol % FEC + 1 wt % AlCl ₃	117 mAh g ⁻¹ (0.1C, 2.0–4.0 V), 81.1% (500 cycles), 1C = 170 mA g ⁻¹	23	
Na _{1.58} Fe[Fe(CN) ₆] _{0.92} nanosphere		hydrothermal	1 M NaPF ₆ in EC/PC (1:1 v/v) + 5% FEC	142 mAh g ⁻¹ (17 mA g ⁻¹ , 2.0–4.2 V), 90% (800 cycles), 1C = 170 mA g ⁻¹	24	

^aDEC, diethyl carbonate; PC, propylene carbonate; EC, ethylene carbonate; FEC, fluoroethylene carbonate; EMS, ethymethanesulfonate.

disordered carbons, along with alloying and conversion materials with appropriate particle size distribution.^{2a,b} Recently, anode-free sodium batteries have garnered widespread attention as their reduced mass would enable the incorporation of more cathode material, which eventually leads to the stable operation of high energy density batteries.³ Further, the cathode component acts as a pivotal and inevitable element for SIB electrochemical performance, which accounts for one-third of the total battery expense.⁴ Therefore, the ideal cathode component must be composed of earth-abundant, nontoxic, highly stable material.

Substantial efforts of various researchers across the globe have resulted in distinct structured SIB cathode materials, for instance, layered transition metal oxide (LTMO), polyanionic compounds, Prussian blue, and its analogues (PBA). These materials contain a certain set of inherent inefficiencies such as inferior conductivity, sluggish kinetics, and severe volume alterations during intercalation–deintercalation cycling which primarily prevents the present-day marketing of SIBs. Therefore, to address these challenges, several mitigation strategies have been adopted including structural modulation, surface modification, and elemental doping, yet the quest for the befitted cathode material persists.

In this short review, we have incorporated the recent advancements of the aforementioned cathode materials and

enumerated their synthetic methods, intrinsic challenges, and upgrading strategies. Further, their commercial aspects and potential candidates for probable future SIB applications have been anticipated. Moreover, the key areas lacking the mechanistic insights among the existing materials have been included for future implementations.

2. OVERVIEW OF CRYSTAL STRUCTURES: CHALLENGES AND STRATEGIES

Exploration of an apt cathode material for Na-ion batteries is an emerging research topic as the massive delving has been experienced by several researchers all over the world, whose efforts contributed to the evolution of the following distinct structured materials whose electrochemical activity has been summarized in Table 1.

2.1. Layered Transition Metal Oxides (LTMOS). The sodium-based layered transition metal oxide with general chemical formula Na_xMO₂ (M = transition metal) exhibits a typical structure comprise of alternatively stacked edge-sharing MO₆ and NaO₆ octahedral layers. These layered materials can further be classified as O3 and P2 according to Delmas' notation depending on the octahedral and prismatic coordination environment of the Na⁺ ion, respectively. Here “2” or “3” depicts the number of transition metal layers with a specific kind of oxygen arrangement. A schematic illustration of

such crystals is shown in Figure 1a,b. Here, the P2 configuration comprises two types of MO₂ layers (AB and

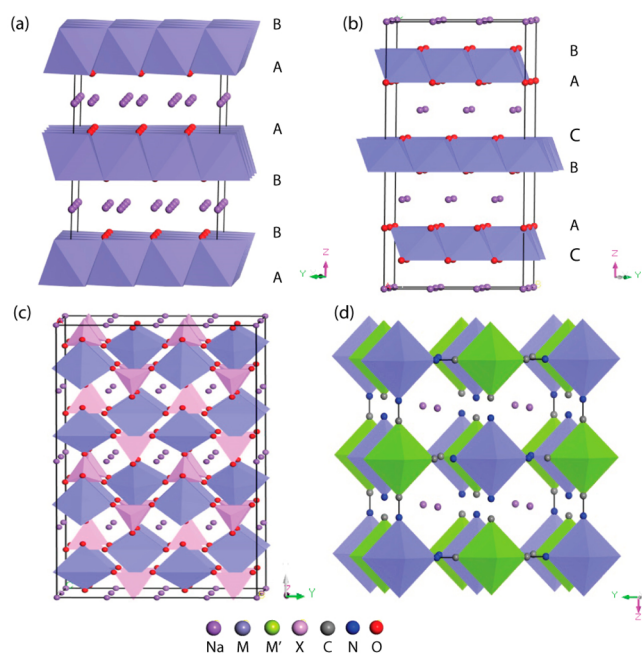
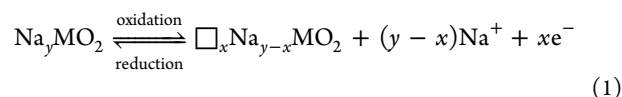


Figure 1. Crystal structures of SIB cathodes: (a) LTMO-P2-Na_{2/3}MO₂, (b) LTMO-O3-NaMO₂, (c) polyanion NaMXO₄, and (d) PBA-NaMM'(CN)₆.

BA), in which all Na ions are located at two kinds of trigonal prismatic sites, namely, Na_f (Na1) and Na_e (Na2), which

comes in contact with two MO₆ octahedra of adjacent slabs along its face and six surrounding MO₆ octahedra along its edges, respectively. On the other hand, in the O3 orientation, Na⁺ ions and 3d transition metals are occupied at different octahedral sites owing to their larger ionic radius difference and are composed of three types of MO₂ slabs, AB, CA, and BC, with distinct oxygen stacking. In addition, in-plane distortion of the crystal lattice is represented by an affixed prime symbol (') like O'3 and P'2. Moreover, extraction of sodium ions from both O3- and P2-type phases can be illustrated by the following equation.



where $y = 1, 0.3 \leq y \leq 0.7$ for O3 and P2 phases, respectively, and \square indicates the created structural vacancy. Generally, sodium insertion–deinsertion from O3 and P2 phases prompts a phase transformation. For the O3-type phase, though Na⁺ ions are stabilized at octahedral sites, sodium deintercalation accompanied the vacancy formation (shown in eq 1), resulting in the generation of energetically stable prismatic sites for Na⁺ ions via the gliding of MO₂ slabs. Consequently, the P3 phase with different oxygen stacking of AB, BC, and CA evolves. Conversely, the orientation of the P2 phase transforms to O2 with AB and AC oxygen layered arrangement during sodium-ion extraction as octahedral sites are created owing to the sliding of MO₂ layers. Therefore, the transition of O3–P3 and P2–O2 exists during the electrochemical cycling, whereas O2 or P2 to O3 or P3 is rather unusual due to the larger energy requirement for M–O bond breakage.

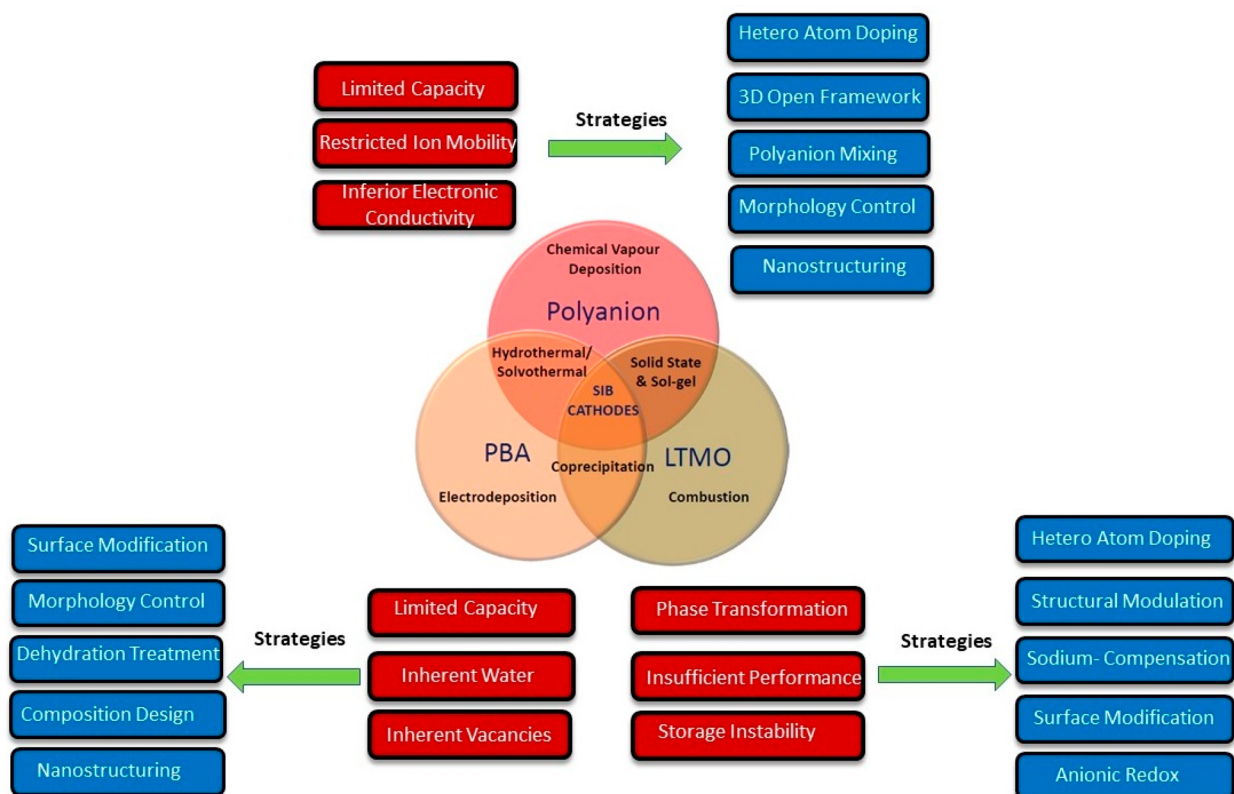


Figure 2. Summary of challenges: mitigation strategies and synthetic protocols of polyanions, LTMO, and PBA materials.

The aforementioned distinct oxygen stacking arrangement results in discrete sodium-ion intercalation sites, leading to different diffusional mechanisms and electrochemical activities. Particularly for O3 structured materials, sodium ions migrate preferably via interstitial tetrahedral sites rather than hopping directly from one octahedral site to another as the former mechanism encounters a lower activation energy barrier in contrast to the latter one. However, in P2-type materials, sodium ions follow a direct passage from one prismatic site to another through an open framework network due to the absence of interstitial tetrahedral sites and experiences a diffusional barrier lower than that of the O3 configuration.

From the electrochemical performance perspective, the P2-type phase could be considered better in contrast to its counter O3 as the spacing between the transition metal layers is larger for the former one, which enables facile Na⁺-ion mobility. Moreover, the P2-type phase maintains its structural integrity due to the minimal transformation (P2–O2), imparting good cycling stability, whereas the O3-type can even undergo a complex phase transition (O3–O'3–P3–P'3–P''3) during the charge–discharge process. However, lower initial sodium content (<2/3) of the P2 phase leads to a reversible capacity relatively lower than that of the O3 arrangement.

Though these materials are considered to be high-capacity cathodes, certain drawbacks like insufficient structural integrity, inadequate storage stability, and sluggish kinetics impede their commercial deployment. Therefore, certain techniques to improve the electrochemical performance of the materials are summarized in Figure 2.

2.1.1. Elemental Doping and Surface Modification.

Further, the accessibility of a wide range of transition elements furnishes these materials with discrete features like plenty of Fe, wide voltage window of Ni, the toxic nature of V and Cr, Mn with high capacity and Jahn–Teller distorting characteristics, high electronic conductivity with expensive Co, structural stability imparting features of electrochemically inactive Mg, Li, Zn, and Al, and air stability inducing behavior of Cu. Extensive studies manifested that the synergistic effect of these elements in terms of heteroatom doping enhances the capacity, cyclability, and stability of the materials. Amidst several structures, P2-type materials exhibit excellent electrochemical performance and high Na⁺-ion mobility and undergo minor phase transformation. Yabuuchi^{5a} et al. in 2012 depicted the synthesis of the binary metal-doped P2-Na_{0.67}Fe_{0.5}Mn_{0.5}O₂ cathode with an initial discharge capacity of 190 mAh g⁻¹ in a 1.5–4.3 V potential window at 12 mA g⁻¹ of current density. Around 72% of its theoretical capacity was attained employing a single electron reaction of Fe³⁺/Fe⁴⁺ and Mn³⁺/Mn⁴⁺ redox couples. For this material, below 3.8 V, Na⁺ ions could be extracted uniformly, while at higher charge voltage, a highly reversible P2-OP4 phase occurred. To further enhance the electrochemical performance, multielement doping has been practiced in recent years. Mu⁶ et al. synthesized an air-stable, Co/Ni-free O3-Na_{0.9}Cu_{0.22}Fe_{0.3}Mn_{0.48}O₂ cathode material which provided around 100 mAh g⁻¹ of specific capacity for a span of over 100 cycles. The reversible O3–P3–P'3 phase transformation along with the contribution of electrochemical active copper (Cu²⁺/Cu³⁺) reinforced the performance of the respective layered oxide. Interestingly, this material demonstrated superior air stability contrary to other reported O3 cathode materials, which might be attributed to the fact of formation of a new surface that protected the bulk material from direct atmospheric contact. Along with elemental doping,

surface modification with oxide coating was devised to resolve the issues associated with atmospheric exposure and electrochemical corrosion. These techniques would help to eradicate HF and moisture content, which ultimately aids the stabilization of the cathode–electrolyte interface. Recently, Alvarado⁷ et al. successfully synthesized Al₂O₃-coated Na_{2/3}Ni_{1/3}Mn_{2/3}O₂ material, which exhibited high Coulombic efficiency and cyclic performance. Prior to coating, a large number of residual salts, organic entities, and esters were observed whose diminished content in the coated electrode enhanced its electrochemical properties.

2.1.2. Structural Modulation. Additionally, for the sake of performance optimization in terms of conductivity, rate capability, and tap density, morphology control came into practice for the construction of microsheets, nanostructures, and radially aligned hierarchical columnar composition. Therefore, to further improve the performance of previously reported P2-Na_{0.67}Fe_{0.5}Mn_{0.5}O₂, the hierarchical nanofibrous structure was prepared using the electrospinning technique followed by calcination.^{5b} The as-prepared material displayed an initial discharge capacity of 195 mAh g⁻¹ due to the shortened Na⁺-ion passage. High-performing cathode materials have also been designed, deploying sol–gel synthetic methodology as a prime tool for obtaining homogenized nanostructured compositions.^{8–10} Additionally, hierarchical columnar structured NaNi_{0.6}Co_{0.05}Mn_{0.35}O₂, synthesized by a coprecipitation method, revealed a much better performance with a preliminary capacity of 157 mAh g⁻¹ at 0.1C compared to that of its bulk counterpart.¹¹ Until now, remarkable contributions have been made for the performance of single phased O3, P2, and P3 structures, but they still fall short due to their intrinsic deficiencies of frequent phase transformations owing to the inevitable gliding of TMO₂ slabs during charge–discharge cycling and insufficient sodium content.

2.1.3. Sodium Compensation. Though the sodium sacrificial salt compensation technique has also been performed, which alleviates the sodium deficiency to some extent, it is not applicable for mass production. Therefore, integrated layer-based composite materials have emerged as they would mitigate the challenges of individual structures and assimilate their advantages to achieve satisfactory sodium-ion storage performance. Recently Yan¹² et al. developed the environmentally stable Co/Ni-free composite P2/P3 Na_{0.78}Cu_{0.27}Zn_{0.06}Mn_{0.67}O₂ material which showed an elevated working voltage of 3.6 V and stable cycling performance for 200 cycles at 0.1C. Here, the Zn substitution urged the intergrowth of P2 and P3 phases, while copper and manganese aided the charge compensation. Moreover, high voltage charging (3.8 V) resulted in the formation of a new phase termed P2_(new) and inhibited the generation of disordered ones.

2.1.4. Anionic Redox. Apart from the conventional cationic redox of transition metals, both Na-deficit and Na-excess materials have showcased the ability to exploit oxygen redox activity as O²⁻/O₂ⁿ⁻ for a charge compensation mechanism. To realize cathodes with enhanced energy density, a technique like the incorporation of alkali metal ions into transition metal layers has been adopted. Recent work by Boisse¹³ et al. displayed the impact of honeycomb cation ordering of a highly stabilized intermediate phase for a Na₂RuO₃ cathode material in instigating the anionic redox activity and providing a capacity of 180 mAh g⁻¹ at 0.2C with a capacity retention of 89% for over 50 cycles. More devoted efforts to realize the

utmost potential of anionic redox ought to be carried out in the future.

2.2. Polyanion Compounds. Primarily the structure of polyanionic materials comprises two entities, namely, MO_x polyhedra ($M = \text{Fe, Mn, Co, etc.}$) and $(\text{XO}_4)_m^{n-}$ or $(\text{X}_m\text{O}_{3m+1})^{n-}$ anionic groups ($X = \text{P, Si, S, etc.}$), which are connected by a corner- or edge-sharing scheme, as shown in Figure 1c. The $(\text{XO}_4)_m^{n-}$ tetrahedron group in polyanionic materials enables the fast alkali ion conduction along with the stabilization of transition metal ion's redox potential. As the oxygen atom is covalently bonded with the transition metal and nonmetallic species, the resulting robust crystal structure possesses higher thermal stability and redox voltage owing to the unique inductive effect of highly electronegative anionic groups compared to their counter layered oxide materials. Nevertheless, these insertion compounds suffer from low conductivity and gravimetric capacity due to the high molecular weight of the polyanion group.¹⁴ Therefore, the investigation of materials with a suitable balance of voltage and capacity is of paramount importance.

To attenuate the inefficacies of the polyanionic materials, corresponding strategies mentioned in Figure 2 have been employed extensively. In general, the performance of the material is greatly influenced by its intrinsic crystal structure; for instance, NaFePO_4 material exhibits polymorphic behavior with olivine and maricite structure. The crystal structure arrangement of the olivine phase consists of PO_4 tetrahedra and FeO_6 octahedra, in which multiple FeO_6 octahedra form a layered structure as they are bridged in a common-point orientation and PO_4 tetrahedra are connected to these layers, generating a one-dimensional channel for Na^+ ion movement. Hence, though the olivine phase is regarded as electrochemically active, it has poor electronic conductivity and low Na^+ ion mobility, making it unable to provide satisfactory performance in its pristine form. Therefore, the induced surface modification via a carbon or conductive polymer coating has been investigated for performance enhancement. Ali^{15a} et al. demonstrated a discharge capacity of 142 mAh g^{-1} within the potential window of 2.2–4.0 V for polythiophene-wrapped olivine NaFePO_4 . The charge–discharge mechanism in $\text{NaFePO}_4/\text{PTh}$ indicated the role of the $\text{Fe}^{2+}/\text{Fe}^{3+}$ redox couple, and variation in unit cell parameters depicted a reversible expansion/contraction phenomenon during sodiation/desodiation cycling.

2.2.1. Nanostructuring. In another polymorph maricite, the FeO_6 octahedron shares edges resulting in 1D chains, while the PO_4 tetrahedra are joined to generate a 3D structure which limits the Na^+ -ion transmission. Even though this structure is considered electrochemically inactive, dimension downsizing would aid its electrochemical performance. Kim^{15b} et al. reported a capacity of 142 mAh g^{-1} at 0.05C for 50 nm sized maricite $\text{Na}_{1-x}\text{FePO}_4$, which is attributed to enhanced sodium mobility due to its amorphous phase transformation. The reaction mechanism illustrated the complete sodium-ion extraction for the high-energy ball-milled maricite NaFePO_4 . After the first deintercalation, the phase transformation of maricite NaFePO_4 to amorphous $\alpha\text{-FePO}_4$ occurred, resulting in a decreased Na^+ -ion energy barrier due to the changed coordination environment of Fe. Although these materials exhibited high capacity, they encountered a large lattice discrepancy and low working potential. Hence, it is unavoidable to explore novel structured materials with large interstitial spaces for smooth Na^+ -ion storage during sodiation

and desodiation cycles. A new iron-based zero-strain $\text{Na}_4\text{Fe}_7(\text{PO}_4)_6$ cathode synthesized via a spray-drying mechanism was reported to exhibit remarkable cyclic stability of 100% capacity retention for over 1000 cycles with a reversible capacity of 66.5 mAh g^{-1} at 54 mA g^{-1} of current density.¹⁶ The as-synthesized material undergoes a solid-solution reaction (single-phase transformation) and indicates the negligible volume variation during intercalation/deintercalation cycling.

2.2.2. 3D Open Framework. Construction of high-dimensional channels for smooth Na^+ -ion mobility would be another route toward achieving high-performance materials. NASICON with the general formula $\text{Na}_3\text{M}_2(\text{XO}_4)_3$ aids this transport by providing a 3D open framework yet further investigations are required to develop a stabilized cathode material in terms of reversibility, longevity, and conductivity. The carbon framework either in terms of coating or support matrix with heteroatom doping serves as an adequate solution to the problem of concern. Chen¹⁷ et al. introduced a 4.0 V N-doped graphene oxide covered $\text{Na}_3\text{V}(\text{PO}_3)_3\text{N}$ composite with consistent carbon-coated NASICON material using a freeze-drying technique, which revealed outstanding cycling stability of 100% capacity retention for over 100 cycles. Topotactic solid-solution reaction depending on single-electron transfer was ascribed for this electrochemical behavior. Next, as the polyanionic materials encounter low specific capacity, the anionic substitution of heavier phosphate group with the lighter electronegative fluorine element would be an apt molecular design engineering solution. Song¹⁸ et al. prepared a fluorophosphate $\text{Na}_3\text{V}_2(\text{PO}_4)_2\text{F}_3$ material deploying the carbothermal reduction method and demonstrated a specific capacity of 111.6 mAh g^{-1} with 97.6% capacity retention for a period of 50 cycles.

Polyanionic materials other than phosphate and pyrophosphates have also been developed using sulfate anionic species. Barpanda^{19a} et al. synthesized an alluaudite structured $\text{Na}_2\text{Fe}_2(\text{SO}_4)_3$ material that presented a high operational voltage of 3.8 V with a decent specific capacity of 100 mAh g^{-1} at 0.05C based on single-phase reaction with nominal volume alterations. Another attempt was made to synthesize an eldefellite $\text{NaFe}(\text{SO}_4)_2$ material using a low-temperature solution route that showed a capacity of 80 mAh g^{-1} with a voltage plateau at 3.3 V.^{19b} Though these materials are based on earth-abundant green Fe element, their practical application is hampered due to their hygroscopic character.

2.2.3. Polyanion Mixing. Further, the combination of various polyanionic groups enables the interesting properties of materials, such as high energy density and strong working voltage. To tune the metal redox, Kim^{20a} et al. synthesized a mixed polyanion via the combination of $(\text{PO}_4)^{3-}$ and $(\text{P}_2\text{O}_7)^{4-}$ groups to provide a 3D framework of the $\text{Na}_4\text{Fe}_3(\text{PO}_4)_2\text{P}_2\text{O}_7$ material with four discernible Na sites out of which three Na^+ ions could be reversibly removed based on $\text{Fe}^{2+}/\text{Fe}^{3+}$ redox and revealed an average voltage of 3.2 V. Recently, to enhance the structural stability and band gap reduction, an isostructural multivalent tetrahedral SiO_4^{4-} substitution for PO_4^{3-} was carried out to obtain $\text{Na}_{3.1}\text{V}_2(\text{PO}_4)_{2.9}(\text{SiO}_4)_{0.1}$ polyanion material using a sol–gel technique. This strategy improved the capacity retention of material up to 98% for 500 cycles.^{20b}

2.3. Prussian Blue Analogues (PBAs). The third thoroughly researched cathode material for SIBs is Prussian blue and its analogues with a general chemical formula of $\text{A}_x\text{M}[\text{M}'(\text{CN})_6](1-y)\cdot n\text{H}_2\text{O}$ ($0 \leq x \leq 2, y \leq 1; \text{A} = \text{Na}^+$),

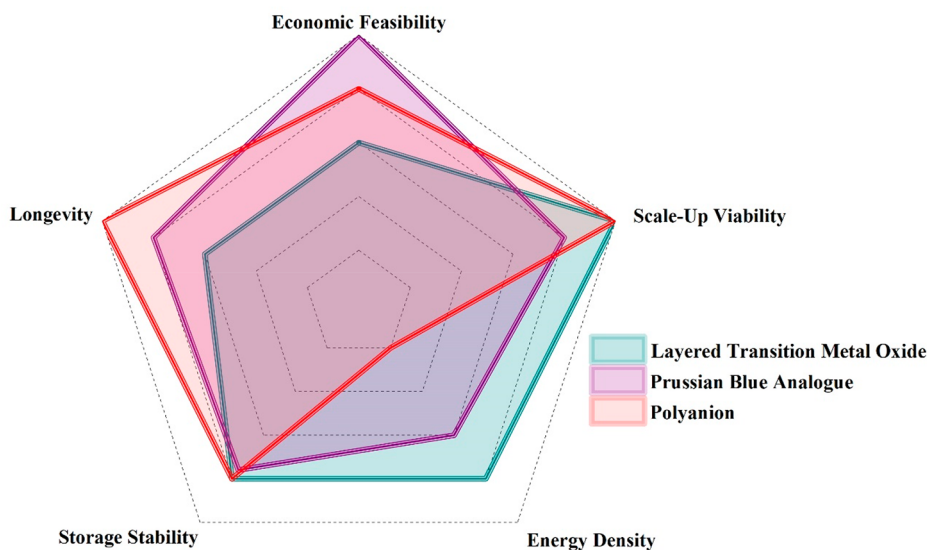
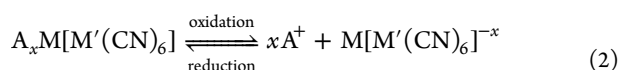


Figure 3. Comparison of existing cathode materials.

where M' is generally occupied by Fe, while M can incorporate a wide variety of transition metals (Co, Cu, Mn, Ni, etc.); \square denotes $[M'(CN)_6]$ vacancies which have an open framework structure with nitrogen and carbon coordinated M' and M cations present high and low spin states, respectively, bonded by cyanide groups, and their crystal structure is illustrated in Figure 1d. Alkali ion concentration influences the crystal structure existence of PBA materials as alkali-deficient ones exhibit cubic structure, whereas alkali-rich prefers a monoclinic configuration. PBAs have captivated the interest of many researchers due to their facile synthetic method, cheap precursors, open framework, and large redox couple. Open channels and interstitial sites aid fast solid-state diffusion of alkali ions in the given structure. The above-stated structure could accommodate up to two alkali ions per unit formula and exhibits electrochemical activity due to the redox reaction of N and C coordinated transition metals, as shown in eq 2.



Further, three discrete forms of water exist in the PBA structures, for instance, surface-adsorbed water, interstitial-containing zeolitic water, and metal-ion-bonded coordinated water. Out of which, the former ones are easier to eliminate compared to the latter due to their physical and chemical interaction with the PBA framework. Though these materials are regarded as promising candidates, their intrinsic problems associated with vacancies and coordinated water result in poor capacity and rate activity, which indeed obstruct their practical utilization. PBA encounters this detrimental effect because sodium-ion transportation gets inhibited due to the presence of water molecules at the interstitial sites of structures, leading to the deterioration of cycling performance. Further, the existence of $[M'(CN)_6]$ vacancies results in lattice distortion and eventual collapse of the structure.

Substantive work has been done for Fe- and Mn-based PBAs as Fe is cheaply available, yet the PBAs based on Fe experience low energy density, whereas Mn-based compounds proffer high operational voltage but are still retarded by their Jahn–Teller distortion effect.

2.3.1. Dehydration Treatment. As water is undesired for nonaqueous batteries, like SIBs, its incorporation during either material synthesis or battery fabrication needs to be reduced. Although infused water in the PBA framework remains stable in ambient conditions, it undergoes dissociation during electrochemical cycling, resulting in performance degradation. Therefore, to eliminate this unprompted water, Goodenough's group proposed a postdehydration technique using high vacuum and low-temperature heating.²¹ In 2015, Wang²² et al. prepared $Na_{1.92}Fe_2(CN)_6$ material with minimal water composition of 0.08 H_2O per formula unit using the solution and subsequent washing route. The charge–discharge profile of the material showcased two voltage plateaus, which existed due to the reaction of disparate Fe spin states and revealed high-capacity retention of 80% for over 1000 cycles. Apart from thermal dehydration, several other strategies like composition and surface modification, as discussed in Figure 2, have been employed to boost the reliability of PBA material. Conventional carbon coating is, however, incompatible for PBA as high temperature leads to its thermal disintegration; a fusion of conductive materials like ketjen black, carbon nanotubes, or development of passivation layer, deploying graphene or reduced graphene oxide and conductive polymers, would rather enhance the conductivity and water stability of the analogue materials.

2.3.2. Heteroatom Doping. As an elemental substitution approach tailors the composition and stoichiometric chemistry of the rechargeable battery materials, therefore, to exploit the synergistic effect, multielement-doped $Na_2Mn_{0.15}Co_{0.15}Ni_{0.1}Fe_{0.6}Fe(CN)_6$ PBA was synthesized via a modified coprecipitation technique which exhibited a reversible cubic–rhombohedral phase transformation and depicted a discharge capacity of 117 $mAh\ g^{-1}$ at 0.1C with a capacity retention of 81.1% for over 500 cycles.²³

2.3.3. Morphology Control. Nevertheless, the current sub-micro- or micro-size-assisted morphological PBA materials are being reported as high-performance cathode materials, but to further enhance the rate performance of the materials, morphology-like macro/meso/hollow nanospheres ought to be developed to shorten the diffusion passage and enable smooth Na^+ -ion intercalation and deintercalation. Conse-

quently, Tang²⁴ et al. prepared a hierarchical $\text{Na}_{1.58}\text{Fe}[\text{Fe}(\text{CN})_6]_{0.92}$ nanosphere via slow reaction between a self-assembled hollow $\text{Fe}^{\text{II}}\text{Ox}$ nanosphere and a $\text{Na}_4\text{Fe}(\text{CN})_6$ precursor. The synthesized material showed a larger surface area and mitigated cell volume alterations during electrochemical cycling compared to those of traditionally reported materials. The designed structure exhibited a specific capacity of 142 mAh g^{-1} at 17 mA g^{-1} current density based on the intercalation of ~ 1.5 Na-ion formula unit and retained 90% of its capacity for over 800 cycles.

3. SUMMARY AND OUTLOOK

3.1. Comparison among Available Cathode Materials.

As the selection of suitable cathode material is the prerequisite of successful SIBs, the following five parameters are considered to scrutinize the material's practical applicability, and the result of each specification is demonstrated in Figure 3 for the corresponding selected materials.

3.1.1. Scale-Up Viability. Active material's scale-up potential is governed by the ease of synthetic method and environmental impact of the corresponding manufacturing process. Though the coprecipitation method appears to be the best option for the commercial application of LTMO and PBA as it is a single-step method and obtains homogeneous solutions, however, the low yield of nanosized PBAs limits their practicality. While the solid-state technique is more suitable for polyanionic material's scale up as it aids high yield and low energy consumption. Moreover, the existing established manufacturing facility of LIBs can be easily transferred to SIB LTMOs to boost their scalability. Further, from the environmental perspective, the usage of toxic V and Cr inhibits the commercialization of LTMOs and polyanionic materials, still, their employment can be curbed by using other nontoxic high valence transition metals, while on the other hand, the release of toxic cyanide at high temperature and acidic conditions invoke a safety concern for PBAs material synthesis. Therefore, LTMOs and polyanionic compounds seem more viable for scale-up application in contrast to PBA materials.

3.1.2. Economic Feasibility. Another factor determining the practical utilization of respective cathodes is economic viability, which is further dictated by the cost of raw materials and post-treatment expenses. As PBAs are primarily based on Fe and Mn, they are considered to be cost-efficient materials, whereas LTMOs are the least preferred ones due to their dependency on expensive Ni, Co, and rare elements for high performance; additional expense of storage and transportation for hygroscopic LTMOs also adds up a surplus amount. Polyanionic materials exhibit an intermediate character as the majority of them are based on rare V element.

3.1.3. Storage Stability. This factor accounts for material stability in atmospheric exposure including moisture and CO_2 contact. Degradation of electrochemical performance of layered oxides arises from the insertion of H_2O or CO_2 , resulting in the formation of inactive NaOH and Na_2CO_3 onto the electrode and generation of an electrically insulating surface. Other materials are also recommended to keep in an inert atmosphere to retain their electrochemical activity. Hence, all materials indicate a rather similar storage characteristic property.

3.1.4. Energy Density. The electrochemical performance of the cathode material is controlled by its specific capacity and redox potential. Layered oxides, particularly O_3 , exhibit high energy density characteristics, whereas the performance of

polyanionic material is affected by its high molecular weight, reducing its specific capacity, ultimately leading to lower energy density. PBAs on the other hand showcase unsatisfactory specific capacity due to the presence of inherent vacancies and coordinated water.

3.1.5. Longevity. The cyclic stability of Polyanionic materials is far larger than its counterpart due to their open 3D framework. While LTMO could sustain its structural integrity only for a very short period of time due to the irreversible phase transformation. PBA material exhibits intermediate behavior due to its robust crystal structure.

In brief, every material has distinct characteristics, and the end application would decide the usage of the respective material, for instance, LTMO appears as an apt candidate for high energy density applications, while PBA would have its implications for longer cyclic operations, and polyanionic materials, on the other hand, would be fitting for high-voltage consumption purposes.^{25a-d}

Furthermore, the most probable potential candidates for grid-scale energy storage requirements in the upcoming years would be $\text{O}_3\text{-Na}_{0.9}\text{Cu}_{0.22}\text{Fe}_{0.30}\text{Mn}_{0.48}\text{O}_2$, $\text{P}_2\text{-Na}_{2/3}\text{Fe}_{1/2}\text{Mn}_{1/2}\text{O}_2$, $\text{Na}_x\text{Fe}[\text{Fe}(\text{CN})_6]$, and $\text{Na}_4\text{Fe}_3(\text{PO}_4)_2\text{P}_2\text{O}_7$, as these materials are based on a facile synthetic method, are earth-abundant nontoxic elements, composed of high electronegative entities, and possess sufficient sodium-ion reservoirs.

3.2. Prototypes for SIB Commercialization. The need for SIB development has engrossed leading industrial organizations beyond academic institutions into paving a sustainable growth path for recognizing the large-scale energy requirements. Multiple companies have addressed this cause and attempted to generate prototypes assisting SIB commercialization by deploying distinct cathode materials while keeping hard carbon as their complementary anode.

In 2015, FARADION fabricated a 3 Ah pouch cell using multielement-doped $\text{Na}_x\text{Ni}_{1-x-y-z}\text{Mn}_x\text{Mg}_y\text{Ti}_z\text{O}_2$ cathode material for powering an electric bicycle.^{25d} Later, SHARP Laboratories Ltd., Europe fabricated a sodium pouch cell utilizing $\text{O}_3\text{-NaNi}_{1/3}\text{Fe}_{1/6}\text{Mn}_{1/3}\text{Mg}_{1/12}\text{Sn}_{1/12}\text{O}_2$ as the cathode material, which exhibited a 94% capacity retention for 150 cycles.^{25e} Furthermore, the first cylindrical cell 18650 type was demonstrated by The French National Centre of Scientific Research (CNRS) and Research Network on Electrochemical Energy Storage (RS2E) employing $\text{Na}_3\text{V}_2(\text{PO}_4)_2\text{F}_3$ as the cathode material, denoting an energy density of 90 Wh kg^{-1} for a continuous 2000 cycles.^{25d} Next, in 2018, NOVASIS Energies Inc. synthesized a batch of 100 kg of PBA material and assembled the pouch cell, which delivered capacity retention of around 98.6% for a span of 500 cycles.^{25f} Recently, a California-based startup, Natron Energy, raised \$35 million for the sole purpose of developing an efficient sodium-ion battery using PBA as its cathode material due to its eco-friendly nature and cost-effective behavior. More recently, Contemporary Amperex Technology Co., Ltd. (CATL) unveiled its first-generation sodium-ion battery utilizing Prussian white as the cathode material and demonstrated an energy density of up to 160 Wh kg^{-1} with their full cell for accomplishing the aim of carbon neutrality.

3.3. Future Prospects. Several strategies have been discerned to attain the satisfactory electrochemical performance for prevailing cathode materials as explained in previous sections, even then the in-depth material understanding, and novel upgrading techniques are still required to mitigate the

existing loopholes and acknowledge the commercial aspects of the respective materials.

For instance, although heteroatom doping has been adopted for performance improvement of every kind of cathode material, still it is imperative to unravel its significance in terms of the appropriate dopant content for the precise active site in the host material. Furthermore, the collaborative effect of multielement doping ought to be corroborated for electrode fabrication. In addition, various facets of heterostructured composite materials remain uncertain, like the requirement of a reasonable ratio adjustment among different structures. Nonetheless, the large surface area of hollow nanostructured materials and low volumetric energy density impair the practical application which could be resolved by the fabrication of multishelled structures, yet the insufficient electro-mechanical understanding obstructs wide-scale application. Furthermore, the recent discovery of anionic redox contribution toward the charge compensation of materials has attracted a lot of attention, still, the inadequate understanding of the exact mechanism garners an ambiguous perception over the proposed concept.


Though the current review highlights cases employing metallic sodium as a counter electrode for the sodium metal cell yet the performance difference between the half and full cell is well established. Therefore, besides the development of efficient cathode materials, other aspects such as the evolution of complementary anode and high-voltage compatible electrolytes, electrolyte additive, selection of suitable binder and separator, and appropriate operational conditions are indispensable. Individual components would have their impact on the overall performance of the entire battery system, for instance, chosen anodes, electrolytes, and separators determine the energy density, safety, stability, and ionic conductivity aspects. Therefore, their compatibility with the cathode requires due attention and must be addressed in the near future to fabricate a commercially viable sodium-ion battery.

Apart from the strategic material designing, characterization techniques to evaluate the phase transformation, structural change, and charge compensation mechanism for Na-ion storage play a vital role in gaining the fundamental understanding of respective SIB materials. For crystal structure evolution, researchers are practicing an integrated approach of X-ray diffraction in situ and ex situ measurements. As the number of transferred electrons by transition metals directly correlate with the amount of deintercalated Na ions, determination of the valence states of the metals in the pristine and electrochemically transformed electrodes is critical for the examination of the charge storage process, especially for multielement electrode materials. Therefore, the X-ray absorption near-edge structure spectroscopy technique has been adopted to calibrate and acknowledge an element's valence states. Additionally, other characterizations such as X-ray photoelectron spectroscopy and Mössbauer spectroscopy are deployed to govern the electronic arrangement, valence state, and coordination environment of SIB electrode materials. Further, researchers should perform in situ/operando experiments as they provide information regarding the component change such as solid–electrolyte interphase formation and solid-state alkali ion diffusion under or close to a working environment.^{26a,b} Moreover, future work should focus on experimental and computational simulations jointly to combine the electrochemical and non-electrochemical analysis for comprehending the mechanistic insight of the respective

concept and establish accurate cell performance measuring parameters.

■ AUTHOR INFORMATION

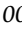
Corresponding Author

Suddhasatwa Basu – Department of Chemical Engineering, Indian Institute of Technology, Delhi 110016, India; CSIR-Institute of Minerals and Materials Technology, Bhubaneswar 751013, India;  orcid.org/0000-0001-7288-2370; Email: sbasu@chemical.iitd.ernet.in

Authors

Priyanka Gupta – Department of Chemical Engineering, Indian Institute of Technology, Delhi 110016, India

Sujatha Pushpakanth – Bharat Forge Limited, Pune 411036, India

M. Ali Haider – Department of Chemical Engineering, Indian Institute of Technology, Delhi 110016, India;  orcid.org/0000-0002-8885-5454

Complete contact information is available at:

<https://pubs.acs.org/10.1021/acsomega.1c05794>

Notes

The authors declare no competing financial interest.

Biographies



Priyanka Gupta received her Bachelor's degree from NIT Srinagar, in the Chemical Engineering discipline as a Gold Medallist. Prior to joining IIT Delhi, she worked as a Senior Engineer-Operations at Vedanta Limited, Goa. Currently, she is pursuing her Ph.D. degree from IIT Delhi in Prof. Suddhasatwa Basu and Prof. M. Ali Haider's group under the Prime Minister's Fellowship Scheme for Doctoral Research. Her research interest includes the synthesis and characterization of electrode materials for sodium-ion battery applications.



Dr. Sujatha Pushpakanth is the Vice-President and Technical Director, Bharat Forge Ltd., Pune, India, and has 25.5 years of experience in diverse verticals like Business & Project Management, New Product Development, Research & Development and Quality Assurance sector of leading industries. She received her Ph.D. degree from the University of Madras, India. She has contributed immensely to developing patented technologies (filed four U.S. patents, granted 1, and 18 Indian Patents, granted 4) for the respective organizations and has received several awards, as well.



Prof. M. Ali Haider completed his M.S. and Ph.D. in Chemical Engineering at the University of Virginia and B. Tech from Indian Institute of Technology (IIT) Guwahati. He joined the Department of Chemical Engineering at IIT Delhi in 2013. He visited the Catalysis Center for Energy Innovation at the University of Delaware in 2017. His research interests are focused on experimental and density functional theory (DFT) based theoretical heterogeneous catalysis applied to the development of biorenewable fuels/chemicals, fuel cells, and batteries. He is a recipient of the Amar Dye-Chem Award for “Excellence in Basic Research and Development in Chemical Engineering” by the Indian Institute of Chemical Engineers, “Bioenergy-Award for Cutting Edge Research” by the Indo–U.S. Science and Technology Forum, DAE-BRNS Young Scientist Award, Gandhian Young Technological Innovation Award, and Institution of Engineers (India) Young Engineers Award. At IIT Delhi, his contributions in teaching and research are noted as “Industry Relevant Best Ph.D. Thesis Supervision”, “Teaching Excellence Award”, and “Early Career Research Award”.



Prof. Suddhasatwa Basu completed Ph.D. in Chemical Engineering from Indian Institute of Science, Bangalore. Prior to taking over as the Director of CSIR-IMMT, he was Professor and Head of Chemical Engineering Department, IIT Delhi. He has vast work experience on development of Energy Materials and its applications to energy conversion and storage devices, e.g., Fuel Cells, Supercapacitor and

Battery, Electrolyser for Hydrogen generation by Water Splitting and CO₂ Reduction to Organics. He has published more than 200 articles in high impact journals with H-index 40, 9 patents and 2 technologies transferred to various industries. He is a fellow of National Academy of Science of India, Indian National Academy of Engineering, Royal Society of Chemistry UK and received Herdillia Award, Dr. A. V. Rama Rao Foundation’s Research Award. He is Editor/Assoc. Editor/Ed. Board member of several international journals published by Wiley, Springer, Elsevier, and ACS.

■ ACKNOWLEDGMENTS

The authors express gratitude towards IIT Delhi (Centre of Excellence-Energy Storage Platform on Batteries), Department of Science and Technology (DST), Science and Engineering Research Board (SERB), Government of India, Confederation of Indian Industry (CII) and partnering company Bharat Forge Ltd. for providing the financial support under the Prime Minister’s Fellowship Scheme for Doctoral Research.

■ REFERENCES

- (1) (a) Dunn, B.; Kamath, H.; Tarascon, J. M. Electrical Energy Storage for the Grid: A Battery of Choices. *Science* **2011**, 928–935. (b) Xie, J.; Song, Y.-W.; Li, B.-Q.; Peng, H.-J.; Huang, J.-Q.; Zhang, Q. Direct Intermediate Regulation Enabled by Sulfur Containers in Working Lithium–Sulfur Batteries. *Angew. Chem.* **2020**, 132 (49), 22334–22339. (c) Liu, X.; He, Q.; Yuan, H.; Yan, C.; Zhao, Y.; Xu, X.; Huang, J. Q.; Chueh, Y. L.; Zhang, Q.; Mai, L. Interface Enhanced Well-Dispersed Co₉S₈ Nanocrystals as an Efficient Polysulfide Host in Lithium–Sulfur Batteries. *J. Energy Chem.* **2020**, 48, 109–115. (d) Xie, J.; Peng, H.; Song, Y.; Li, B.; Xiao, Y.; Zhao, M.; Yuan, H.; Huang, J.; Zhang, Q. Spatial and Kinetic Regulation of Sulfur Electrochemistry on Semi-Immobilized Redox Mediators in Working Batteries. *Angew. Chem.* **2020**, 132 (40), 17823–17828.
- (2) (a) Chandra, M.; Khan, T. S.; Shukla, R.; Ahamad, S.; Gupta, A.; Basu, S.; Haider, M. A.; Dhaka, R. S. Diffusion Coefficient and Electrochemical Performance of NaVO₃ Anode in Li/Na Batteries. *Electrochim. Acta* **2020**, 331, 135293. (b) Chen, X.; Bai, Y. K.; Shen, X.; Peng, H. J.; Zhang, Q. Sodiophilicity/Potassiophilicity Chemistry in Sodium/Potassium Metal Anodes. *J. Energy Chem.* **2020**, 51, 1–6.
- (3) Tanwar, M.; Bezabh, H.; Basu, S.; Su, W.-N.; Hwang, B.-J. Investigation of Sodium Plating and Stripping on a Bare Current Collector with Different Electrolytes and Cycling Protocols. *ACS Appl. Mater.* **2019**, 11 (43), 39746–39756.
- (4) Kim, Y.; Ha, K. H.; Oh, S. M.; Lee, K. T. High-Capacity Anode Materials for Sodium-Ion Batteries. *Chem.-Eur. J.* **2014**, 11980–11992.
- (5) (a) Yabuuchi, N.; Kajiyama, M.; Iwatate, J.; Nishikawa, H.; Hitomi, S.; Okuyama, R.; Usui, R.; Yamada, Y.; Komaba, S. P2-Type Na_x[Fe_{1/2}Mn_{1/2}O₂] Made from Earth-Abundant Elements for Rechargeable Na⁺ Batteries. *Nat. Mater.* **2012**, 11 (6), 512–517. (b) Kalluri, S.; Seng, K. H.; Pang, W. K.; Guo, Z.; Chen, Z.; Liu, H.-K.; Dou, S. X. Electrospun P2-Type Na_{2/3}(Fe_{1/2}Mn_{1/2})O₂ Hierarchical Nanofibers as Cathode Material for Sodium-Ion Batteries. *ACS Appl. Mater. Interfaces* **2014**, 6 (12), 8953–8958.
- (6) Mu, L.; Xu, S.; Li, Y.; Hu, Y. S.; Li, H.; Chen, L.; Huang, X. Prototype Sodium-Ion Batteries Using an Air-Stable and Co/Ni-Free O₃-Layered Metal Oxide Cathode. *Adv. Mater.* **2015**, 27 (43), 6928–6933.
- (7) Alvarado, J.; Ma, C.; Wang, S.; Nguyen, K.; Kodur, M.; Meng, Y. S. Improvement of the Cathode Electrolyte Interphase on P2-Na_{2/3}Ni_{1/3}Mn_{2/3}O₂ by Atomic Layer Deposition. *ACS Appl. Mater. Interfaces* **2017**, 9 (31), 26518–26530.
- (8) Saroha, R.; Khan, T. S.; Chandra, M.; Shukla, R.; Panwar, A. K.; Gupta, A.; Haider, M. A.; Basu, S.; Dhaka, R. S. Electrochemical Properties of Na_{0.66}V₄O₁₀ Nanostructures as Cathode Material in Rechargeable Batteries for Energy Storage Applications. *ACS Omega* **2019**, 4 (6), 9878–9888.

- (9) Chandra, M.; Shukla, R.; Saroha, R.; Panwar, A. K.; Gupta, A.; Basu, S.; Dhaka, R. S. Physical Properties and Electrochemical Performance of Zn-Substituted $\text{Na}_{0.44}\text{Mn}_{1-x}\text{Zn}_x\text{O}_2$ Nanostructures as Cathode in Na-Ion Batteries. *Ceram. Int.* **2018**, *44* (17), 21127–21131.
- (10) Chandra, M.; Shukla, R.; Rashid, M.; Gupta, A.; Basu, S.; Dhaka, R. S. Synthesis and Physical Properties of Na_xTO_2 ($T = \text{Mn, Co}$) Nanostructures for Cathode Materials in Na-Ion Batteries. *Mater. Res. Bull.* **2018**, *105*, 178–183.
- (11) Hwang, J. Y.; Oh, S. M.; Myung, S. T.; Chung, K. Y.; Belharouak, I.; Sun, Y. K. Radially Aligned Hierarchical Columnar Structure as a Cathode Material for High Energy Density Sodium-Ion Batteries. *Nat. Commun.* **2015**, *6* (1), 1–9.
- (12) Yan, Z.; Tang, L.; Huang, Y.; Hua, W.; Wang, Y.; Liu, R.; Gu, Q.; Indris, S.; Chou, S. L.; Huang, Y.; Wu, M.; Dou, S. X. A Hydrostable Cathode Material Based on the Layered P2@P3 Composite That Shows Redox Behavior for Copper in High-Rate and Long-Cycling Sodium-Ion Batteries. *Angew. Chemie - Int. Ed.* **2019**, *58* (5), 1412–1416.
- (13) Mortemard De Boisse, B.; Liu, G.; Ma, J.; Nishimura, S. I.; Chung, S. C.; Kiuchi, H.; Harada, Y.; Kikkawa, J.; Kobayashi, Y.; Okubo, M.; Yamada, A. Intermediate Honeycomb Ordering to Trigger Oxygen Redox Chemistry in Layered Battery Electrode. *Nat. Commun.* **2016**, *7* (1), 1–9.
- (14) Sapra, S. K.; Pati, J.; Dwivedi, P. K.; Basu, S.; Chang, J.-K.; Dhaka, R. S. A Comprehensive Review on Recent Advances of Polyanionic Cathode Materials in Na-Ion Batteries for Cost Effective Energy Storage Applications. *Wiley Interdiscip. Rev. Energy Environ.* **2021**, *10* (5), No. e400.
- (15) (a) Ali, G.; Lee, J. H.; Susanto, D.; Choi, S. W.; Cho, B. W.; Nam, K. W.; Chung, K. Y. Polythiophene-Wrapped Olivine NaFePO_4 as a Cathode for Na-Ion Batteries. *ACS Appl. Mater. Interfaces* **2016**, *8* (24), 15422–15429. (b) Kim, J.; Seo, D.-H.; Kim, H.; Park, I.; Yoo, J.-K.; Jung, S.-K.; Park, Y.-U.; Goddard III, W. A.; Kang, K. Unexpected Discovery of Low-Cost Maricite NaFePO_4 as a High-Performance Electrode for Na-Ion Batteries. *Energy Environ. Sci.* **2015**, *8* (2), 540–545.
- (16) Pu, X.; Rong, C.; Tang, S.; Wang, H.; Cao, S.; Ding, Y.; Cao, Y.; Chen, Z. Zero-Strain $\text{Na}_4\text{Fe}_7(\text{PO}_4)_6$ as a Novel Cathode Material for Sodium-Ion Batteries. *Chem. Commun.* **2019**, *55* (61), 9043–9046.
- (17) Chen, M.; Hua, W.; Xiao, J.; Cortie, D.; Guo, X.; Wang, E.; Gu, Q.; Hu, Z.; Indris, S.; Wang, X. L.; Chou, S. L.; Dou, S. X. Development and Investigation of a NASICON-Type High-Voltage Cathode Material for High-Power Sodium-Ion Batteries. *Angew. Chemie - Int. Ed.* **2020**, *59* (6), 2449–2456.
- (18) Song, W.; Ji, X.; Wu, Z.; Yang, Y.; Zhou, Z.; Li, F.; Chen, Q.; Banks, C. E. Exploration of Ion Migration Mechanism and Diffusion Capability for $\text{Na}_3\text{V}_2(\text{PO}_4)_2\text{F}_3$ Cathode Utilized in Rechargeable Sodium-Ion Batteries. *J. Power Sources* **2014**, *256*, 258–263.
- (19) (a) Barpanda, P.; Oyama, G.; Nishimura, S. I.; Chung, S. C.; Yamada, A. A 3.8-V Earth-Abundant Sodium Battery Electrode. *Nat. Commun.* **2014**, *5* (1), 1–8. (b) Singh, P.; Shiva, K.; Celio, H.; Goodenough, J. B. $\text{NaFe}(\text{SO}_4)_2$: An Intercalation Cathode Host for Low-Cost Na-Ion Batteries. *Energy Environ. Sci.* **2015**, *8* (10), 3000–3005.
- (20) (a) Kim, H.; Park, I.; Seo, D. H.; Lee, S.; Kim, S. W.; Kwon, W. J.; Park, Y. U.; Kim, C. S.; Jeon, S.; Kang, K. New Iron-Based Mixed-Polyanion Cathodes for Lithium and Sodium Rechargeable Batteries: Combined First Principles Calculations and Experimental Study. *J. Am. Chem. Soc.* **2012**, *134* (25), 10369–10372. (b) Wang, M.; Guo, J.-Z.; Wang, Z.-W.; Gu, Z.-Y.; Nie, X.-J.; Yang, X.; Wu, X.-L. Isostructural and Multivalent Anion Substitution toward Improved Phosphate Cathode Materials for Sodium-Ion Batteries. *Small* **2020**, *16* (16), 1907645.
- (21) Song, J.; Wang, L.; Lu, Y.; Liu, J.; Guo, B.; Xiao, P.; Lee, J.-J.; Yang, X.-Q.; Henkelman, G.; Goodenough, J. B. Removal of Interstitial H_2O in Hexacyanometallates for a Superior Cathode of a Sodium-Ion Battery. *J. Am. Chem. Soc.* **2015**, *137* (7), 2658–2664.
- (22) Wang, L.; Song, J.; Qiao, R.; Wray, L. A.; Hossain, M. A.; Chuang, Y. De; Yang, W.; Lu, Y.; Evans, D.; Lee, J. J.; Vail, S.; Zhao, X.; Nishijima, M.; Kakimoto, S.; Goodenough, J. B. Rhombohedral Prussian White as Cathode for Rechargeable Sodium-Ion Batteries. *J. Am. Chem. Soc.* **2015**, *137* (7), 2548–2554.
- (23) Xie, B.; Zuo, P.; Wang, L.; Wang, J.; Huo, H.; He, M.; Shu, J.; Li, H.; Lou, S.; Yin, G. Achieving Long-Life Prussian Blue Analogue Cathode for Na-Ion Batteries via Triple-Cation Lattice Substitution and Coordinated Water Capture. *Nano Energy* **2019**, *61*, 201–210.
- (24) Tang, X.; Liu, H.; Su, D.; Notten, P. H. L.; Wang, G. Hierarchical Sodium-Rich Prussian Blue Hollow Nanospheres as High-Performance Cathode for Sodium-Ion Batteries. *Nano Res.* **2018**, *11*, 3979.
- (25) (a) Li, W. J.; Han, C.; Wang, W.; Gebert, F.; Chou, S. L.; Liu, H. K.; Zhang, X.; Dou, S. X. Commercial Prospects of Existing Cathode Materials for Sodium Ion Storage. *Adv. Energy Mater.* **2017**, *7* (24), 1700274. (b) Yabuuchi, N.; Kubota, K.; Dahbi, M.; Komaba, S. Research Development on Sodium-Ion Batteries. *Chem. Rev.* **2014**, *114* (23), 11636–11682. (c) Dai, Z.; Mani, U.; Tan, H. T.; Yan, Q. Advanced Cathode Materials for Sodium-Ion Batteries: What Determines Our Choices? *Small Methods* **2017**, *1* (5), 1700098. (d) Delmas, C. Sodium and Sodium-Ion Batteries: 50 Years of Research. *Adv. Energy Mater.* **2018**, *8* (17), 1703137. (e) Smith, K.; Treacher, J.; Ledwoch, D.; Adamson, P.; Kendrick, E. Novel High Energy Density Sodium Layered Oxide Cathode Materials: From Material to Cells. *ECS Trans.* **2017**, *75* (22), 13–24. (f) Bauer, A.; Song, J.; Vail, S.; Pan, W.; Barker, J.; Lu, Y. The Scale-up and Commercialization of Nonaqueous Na-Ion Battery Technologies. *Adv. Energy Mater.* **2018**, *8* (17), 1702869.
- (26) (a) Zeng, Z.; Barai, P.; Lee, S. Y.; Yang, J.; Zhang, X.; Zheng, W.; Liu, Y. S.; Bustillo, K. C.; Ercius, P.; Guo, J.; Cui, Y.; Srinivasan, V.; Zheng, H. Electrode Roughness Dependent Electrodeposition of Sodium at the Nanoscale. *Nano Energy* **2020**, *72*, 104721. (b) Zeng, Z.; Liang, W. I.; Liao, H. G.; Xin, H. L.; Chu, Y. H.; Zheng, H. Visualization of Electrode-Electrolyte Interfaces in $\text{LiPF}_6/\text{EC}/\text{DEC}$ Electrolyte for Lithium Ion Batteries via in Situ TEM. *Nano Lett.* **2014**, *14* (4), 1745–1750.